Contribution of isotopologue self-shielding to sulfur mass-independent fractionation during sulfur dioxide photolysis

Citation: Ono, S., A. R. Whitehill, and J. R. Lyons. "Contribution of Isotopologue Self-Shielding to Sulfur Mass-Independent Fractionation During Sulfur Dioxide Photolysis." Journal of Geophysical Research: Atmospheres 118, no. 5 (March 16, 2013): 2444–2454. Copyright © 2013 American Geophysical Union

As Published: http://dx.doi.org/10.1002/jgrd.50183

Persistent URL: http://hdl.handle.net/1721.1/85603

Version: Final published version: final published article, as it appeared in a journal, conference proceedings, or other formally published context

Contribution of isotopologue self-shielding to sulfur mass-independent fractionation during sulfur dioxide photolysis

S. Ono,[1] A. R. Whitehill,[1] and J. R. Lyons[2]

Received 12 October 2012; revised 28 December 2012; accepted 9 January 2013; published 12 March 2013.

[1] Signatures of sulfur mass-independent fractionation (S-MIF) are observed for sulfur minerals in Archean rocks, and for modern stratospheric sulfate aerosols (SSA) deposited in polar ice. Ultraviolet light photolysis of SO_2 is thought to be the most likely source for these S-MIF signatures, although several hypotheses have been proposed for the underlying mechanism(s) of S-MIF production. Laboratory SO_2 photolysis experiments are carried out with a flow-through photochemical reactor with a broadband (Xe arc lamp) light source at 0.1 to 5 mbar SO_2 in 0.25 to 1 bar N_2 bath gas, in order to test the effect of SO_2 pressure on the production of S-MIF. Elemental sulfur products yield high $\delta^{34}S$ values up to 140 ‰, with $\delta^{33}S/\delta^{34}S$ of 0.59 ± 0.04 and $\Delta^{36}S/\Delta^{33}S$ ratios of -4.6 ± 1.3 with respect to initial SO_2. The magnitude of the isotope effect strongly depends on SO_2 partial pressure, with larger fractionations at higher SO_2 pressures, but saturates at an SO_2 column density of 10^{18} molecules cm^{-2}. The observed pressure dependence and $\delta^{33}S/\delta^{34}S$ and $\Delta^{36}S/\Delta^{33}S$ ratios are consistent with model calculations based on synthesized SO_2 isotopologue cross sections, suggesting a significant contribution of isotopologue self-shielding to S-MIF for high SO_2 pressure (>0.1 mbar) experiments. Results of dual-cell experiments further support this conclusion. The measured isotopic patterns, in particular the $\Delta^{36}S/\Delta^{33}S$ relationships, closely match those measured for modern SSA from explosive volcanic eruptions. These isotope systematics could be used to trace the chemistry of SSA after large Plinian volcanic eruptions.

Citation: Ono, S., A. R. Whitehill, and J. R. Lyons (2013), Contribution of isotopologue self-shielding to sulfur mass-independent fractionation during sulfur dioxide photolysis, *J. Geophys. Res. Atmos.*, *118*, 2444–2454, doi:10.1002/jgrd.50183.

1. Introduction

[2] Sulfate and sulfide minerals in sedimentary rocks older than 2.4 Giga years ago (Ga) commonly show signatures of sulfur isotope mass-independent fractionation (S-MIF), anomalous isotope compositions that deviate from the mass-dependent scaling law of isotope fractionation [e.g., *Farquhar et al*., 2000a; *Pavlov and Kasting*, 2002; *Ono et al*., 2003]. Equilibrium, kinetic, and biological processes nominally fractionate four stable isotopes of sulfur (^{32}S, ^{33}S, ^{34}S, and ^{36}S) in proportion to their difference in mass as predicted by the quantum mechanical theory of isotope fractionation [e.g., *Urey*, 1947]. Therefore, the preservation of MIF signatures indicate that a fundamental change in the sulfur cycle occurred at about 2.4 Ga. Assuming that the MIF signature is sourced from ultraviolet (UV) photolysis of SO_2, production and preservation of S-MIF signatures are thought to only be possible under an anoxic early atmosphere that is UV transparent and allows rich sulfur atmospheric chemistry [*Farquhar et al*., 2000a, 2001; *Pavlov and Kasting*, 2002]. In addition, several works suggest potential secular structures in the Archean S-MIF record, such as changes in the magnitude of ^{33}S anomaly or in the relationship between the ^{33}S and ^{36}S anomalies [*Ono et al*., 2006a; *Ohmoto et al*., 2006; *Farquhar et al*., 2007; *Zerkle et al*., 2012]. A better understanding of the mechanisms responsible for the production of S-MIF during SO_2 photolysis would provide additional constraints on the early evolution of the atmosphere beyond atmospheric oxygen levels.

[3] S-MIF signatures are also measured in stratospheric sulfate aerosols (SSA) deposited in polar ice [*Savarino et al*., 2003, *Baroni et al*., 2007, 2008]. These S-MIF signatures are only associated with large stratospheric eruptions (e.g., Pinatubo, 1991, Agung, 1963, Tambora, 1815) but not with predominantly tropospheric eruptions (e.g., Cerro Hudson, 1991), suggesting S-MIF can be used as a proxy for stratospheric volcanic events in the past [*Savarino et al*., 2003; *Baroni et al*., 2007, 2008]. The source reaction for S-MIF in the modern stratosphere, however, has been debated, because the MIF source mechanism is still not well constrained, and because of the difficulty in preserving S-MIF signatures in a present-day atmosphere [*Savarino et al*., 2003; *Pavlov et al*., 2005].

[1]Department of Earth, Atmospheric, and Planetary Sciences, Massachusetts Institute of Technology, Cambridge, MA, USA.
[2]Department of Earth and Space Sciences, UCLA, Los Angeles, CA, USA.

Corresponding author: S. Ono, Department of Earth, Atmospheric, and Planetary Sciences, Massachusetts Institute of Technology, Cambridge, MA, USA. (sono@mit.edu)

2169-897X/13/10.1002/jgrd.50183

[4] Laboratory photochemical studies have shown that photolysis of SO_2 and photopolymerization of CS_2 both produce S-MIF [*Farquhar et al.*, 2001; *Masterson et al.*, 2011; *Whitehill and Ono*, 2012; *Zmolek et al.*, 1999], but photolysis of H_2S and OCS does not [*Farquhar et al.*, 2000b; *Lin et al.*, 2011]. Both CS_2 and SO_2 exhibit fine structures in their UV absorption spectrum, suggesting that S-MIF is associated with the process of predissociation [*Farquhar et al.*, 2001; *Zmolek et al.*, 1999; *Danielache et al.*, 2008; *Lyons*, 2007, 2008]. Two absorption bands of SO_2, from 190 to 220 nm and 240 to 340 nm, are thought to be important for S-MIF production [*Farquhar et al.*, 2001; *Danielache et al.*, 2008]. Laboratory experiments by *Farquhar et al.* [2001] showed that the pattern of S-MIF depends on the wavelength of excitation. This was used to link the 190 to 220 nm band to Archean S-MIF [*Farquhar et al.*, 2001; *Ueno et al.*, 2008; *Lyons*, 2007], and the 240 to 340 nm band to the S-MIF in SSA [*Savarino et al.*, 2003; *Baroni et al.*, 2007, 2008]. However, recent work using broadband radiation sources shows that S-MIF associated with the 240 to 340 nm is characterized by a positive correlation between $\Delta^{36}S$ and $\Delta^{33}S$ values, whereas negative correlations are observed in SSA [*Whitehill and Ono*, 2012]. Thus, in this study, we focus on the excitation of SO_2 under the 190 to 220 nm absorption region.

[5] Several hypotheses have been proposed for the mechanism underlying the production of S-MIF. A symmetry-dependent isotope effect, which has been suggested as the mechanism for oxygen isotope MIF during the ozone recombination reaction [*Gao and Marcus*, 2001], does not apply to SO_2, as sulfur isotope substitution does not change the molecular symmetry of SO_2. The SO_2 absorption band in the 190 to 220 nm region exhibits vibrational fine structure due to bending mode progressions of the $^1B_2 \leftarrow X^1A_1$ system (Figure 1-A) [*Freeman et al.*, 1984]. Isotope substitutions shift the band positions and can produce isotope self-shielding due to differential optical column density (Figure 1) [Lyons, 2007, 2008]. In addition to the shift of band positions, sulfur isotope substitution can also affect the cross-section amplitude due to isotope differences in the Franck-Condon envelope and vibrational structures [*Danielache et al.*, 2008; *Tokue and Nanbu*, 2010]. Molecular dynamics during predissociation, such as nonadiabatic resonances among various bound excited states of SO_2, may also contribute to S-MIF production [e.g., *Masterson et al.*, 2011 and *Zmolek et al.*, 1999 for CS_2].

[6] The goal of this study, therefore, is to test which of these three proposed mechanisms contributes predominantly to the observed S-MIF in Archean rocks, SSA, and laboratory photochemical experiments. Previous laboratory photochemical experiments employed static photochemical cells with SO_2 partial pressures (pSO_2) ranging from 6 mbar to over one bar [*Farquhar et al.*, 2001; *Masterson et al.*, 2011; *Whitehill and Ono*, 2012]. Isotopologue self-shielding is expected to take effect under these high SO_2 column densities ($>3.3 \times 10^{19}$ molecules cm^{-2}) [*Lyons*, 2007, 2008]. We used a flow-through photochemical cell to measure S-MIF at pSO_2 as low as 0.1 mbar (corresponding column density at 3.8×10^{16} molecules cm^{-2}), in order to test the contribution of isotopologue self-shielding. In addition, two photochemical cells are placed in series for some experiments to isolate the spectrum effects by only varying pSO_2 of the front cell, while holding pSO_2 of the rear cell constant. The experimental results are compared with isotope fractionation expected from synthetic isotopologue-dependent cross sections by *Lyons* [2007] that account only for the effect of band-position shifts. By experimentally studying the effect of SO_2 pressure, we also aimed to isolate the production of S-MIF by mechanisms other than self-shielding.

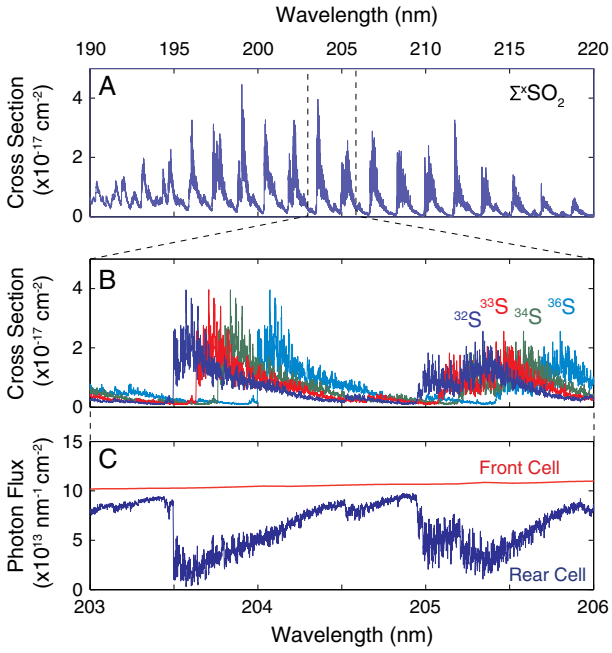

Figure 1. Origin of self-shielding isotope effect. (A) UV absorption cross section of SO_2 for 190 to 220 nm region [*Freeman et al.*, 1984]. (B) Isotopologue specific cross sections in the 203 to 206 nm modeled by red shifting the spectrum of $^{32}SO_2$ [*Lyons*, 2007; 2008]. (C) Estimated photon flux for dual-cell experiments for 2.5mbar pSO_2 for the front cell (column density of 9.4×10^{16} cm^{-2}). The photon absorption is due primarily to $^{32}SO_2$, which constitutes 96% of total SO_2. Although isotope red shifting is mass dependent, differential absorption is abundance dependent such that the conventional mass-dependent law does not apply.

2. Method

2.1. Photochemical Experiments

[7] Photolysis experiments were carried out using a dual-cell flow-through photochemical reactor illustrated in Figure 2. Each cylindrical glass photochemical cell (15 cm length, 5 cm inside diameter) is equipped with two UV grade windows (Corning 7980 grade, > 90% UV transmittance above 190 nm) sealed by o-rings, and inlet and outlet ports (made of 3/8" o.d. glass tubes). For dual-cell experiments, two identical flow-through cells were placed in series. Premixed SO_2–N_2 gas (100 ppm or 5% SO_2) was diluted with pure N_2 (UHP grade) using digital mass flow controllers and flowed continuously through the photochemical cell. Pressure inside the cell was monitored with capacitance manometers (MKS, 1000 torr full scale). The reaction cell was pumped continuously with a diaphragm pump through a needle valve and a vacuum regulator for experiments under pN_2 less than 1 bar. Errors in pSO_2 are estimated to be

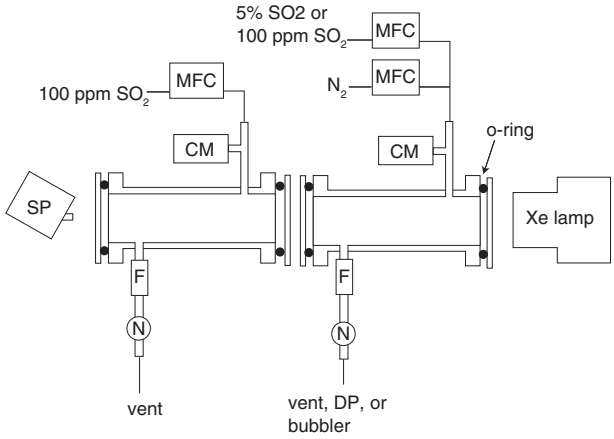

Figure 2. Schematics of the dual-cell flow-through reactor used in this study. MFC: mass flow controller, CM: capacitance manometer, SP: spectrometer, F: glass wool filter, N: needle valve. The outlet of the front photochemical cell (right) is vented, pumped by a diaphragm pump (DP), or sampled for residual SO_2 using a set of bubblers. *See* text for details.

between 5 and 10%, based upon the precision and accuracy of the mass flow controllers and the manometer. A 150 W Xenon arc lamp (Model 6254, Newport) in a lamp housing (Model 67005, Newport) was used as a light source for all experiments. The irradiance spectrum between 190 and 400 nm was monitored with a UV spectrometer (SPM-002-BT, Photon Control, Burnaby, Canada), which was calibrated against Hg lamp lines for wavelength. The Xe arc lamp emits continuum radiation down to at least 190 nm (and possibly lower).

[8] While the excitation of SO_2 by radiation in the 240 to 340 nm region ($^1A_2$, $^1B_1 \leftarrow X\,^1A_1$) occurs in our experiments, the resulting low-energy excited states are rapidly quenched (within 4 to 300 ns for the singlet and triplet states, respectively) by collisions with N_2 before participating in any chemical reactions such as self-reaction with SO_2 [*Sidebottom et al.*, 1972; *Calvert et al.*, 1978; *Whitehill and Ono*, 2012].

[9] UV irradiation of the SO_2 produces elemental sulfur (S^0), sulfur trioxide (SO_3), and residual SO_2 with the overall reaction stoichiometry [*Ustinov et al.*, 1988]:

$$3SO_2 + h\nu \rightarrow 2SO_3 + S^0$$

[10] Upon photolysis, S^0 and SO_3 condensed inside the photochemical cell and on a glass wool filter placed at the outlet port, and were collected by rinsing with dichloromethane and deionized water, respectively. The S^0 was crystallized from dichloromethane by evaporation and reduced to H_2S by Cr reduction and precipitated as Ag_2S by a procedure modified from *Gröger et al.* [2009]. SO_3 rapidly hydrolyzes to sulfate in water and was precipitated as barium sulfate by the addition of a barium chloride solution. For two experiments (S-1020 and S-1021), residual SO_2 was collected by bubbling effluent in a series of two bubblers, the first containing 60 mL of 80% isopropyl alcohol, and the second 60 mL of 3% hydrogen peroxide, to capture SO_3 and residual SO_2, respectively. After photolysis, these trapping solutions were acidified to pH < 4 with 6 N HCl, and sulfate was precipitated as barium sulfate. The first trap did not yield quantifiable (less than 1 mg) $BaSO_4$, suggesting that the majority of the SO_3 was trapped at the glass wool trap or on the walls of the photochemical cell. The barium sulfate was reduced to H_2S and precipitated as Ag_2S by the method described in *Forrest and Newman* [1977].

2.2. Isotope Ratio Analysis

[11] A detailed description of the isotope ratio analysis method can be found in *Ono et al.* [2006b]. Approximately 2 mg of Ag_2S was reacted with elemental fluorine gas in externally heated nickel tubes (at 300 °C) to form SF_6. The product SF_6 is purified by gas chromatography, introduced to a gas source isotope ratio mass spectrometer (MAT 253, Thermo-Fisher), and measured for four ion beams of SF_5^+ ($^{32}SF_5^+$, $^{33}SF_5^+$, $^{34}SF_5^+$, and $^{36}SF_5^+$). A microvolume

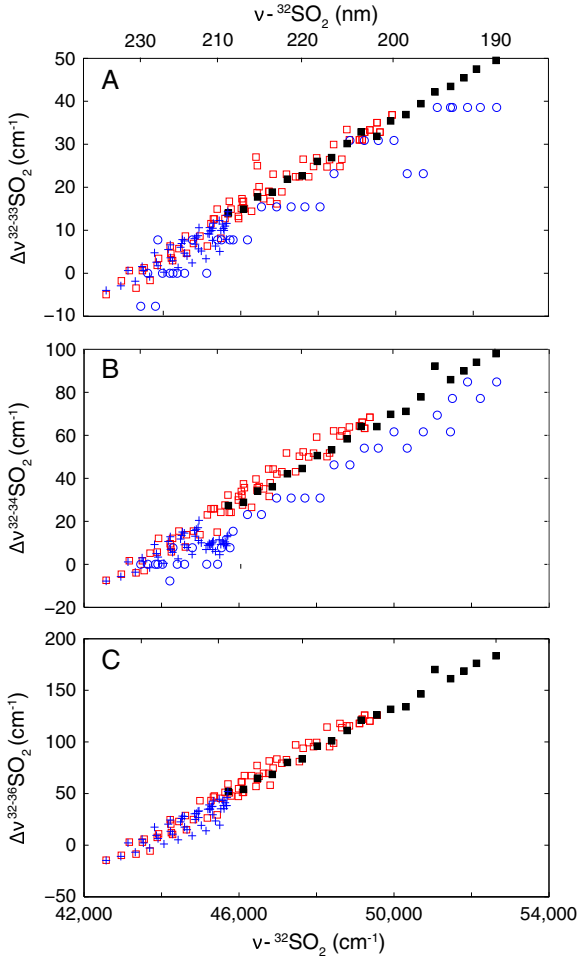

Figure 3. SO_2 isotope shift parameters used in this study [filled square, *Lyons*, 2007; 2008] compared to those derived experimentally [open circle, *Danielache et al.*, 2008] and by ab-initio theoretical modeling [cross, *Ran et al.*, 2007; open square, *Tokue and Nanbu*, 2010]. The energy shifts for isotopologues (in wavenumber cm^{-1}) are plotted against the frequency of $^{32}SO_2$. A, B, and C show the energy shift between $^{32}SO_2$ and $^{33}SO_2$, $^{32}SO_2$ and $^{34}SO_2$, and $^{32}SO_2$ and $^{36}SO_2$, respectively.

(0.4 mL) procedure was used for small samples (<1 mg Ag_2S). Replicate analyses ($N = 28$) of the reference Ag_2S IAEA-S-1 yielded 2σ standard deviations of 0.26‰, 0.014‰, and 0.19‰ for $\delta^{36}S$, $\Delta^{33}S$, and $\Delta^{36}S$, respectively [*Ono et al*., 2012]. Typical reproducibility for microvolume analyses of IAEA-S-1 is 0.9‰, 0.08‰, and 0.8‰ for $\delta^{36}S$, $\Delta^{33}S$, and $\Delta^{36}S$, respectively (2σ for 14 replicate analyses).

[12] Sulfur isotope compositions are reported in conventional δ notation, defined as:

$$\delta^x S = {}^xR_{sa}/{}^xR_i - 1 \quad (1)$$

where ${}^xR$ is the ratio ${}^xS/{}^{32}S$ (x = 33, 34, or 36) of sample (R_{sa}) and initial SO_2 (R_i), respectively. The common multiplication factor of 1000 is omitted because it technically belongs to ‰ symbol [*Coplen*, 2011]. The magnitude of S-MIF is reported using capital delta notations calculated according to:

$$\Delta^{33}S = \left({}^{33}R_{sa}/{}^{33}R_i\right)/\left({}^{34}R_{sa}/{}^{34}R_i\right)^{0.515} - 1, \quad (2)$$

$$\Delta^{36}S = \left({}^{33}R_{sa}/{}^{33}R_i\right)/\left({}^{34}R_{sa}/{}^{34}R_i\right)^{1.90} - 1. \quad (3)$$

[13] We use the definitions above among various definitions because they are mathematically consistent with the δ notation (i.e., deviation of the ratio from the expected ratio) [see *Kaiser et al*., 2004].

2.3. Modeling the Effect of Isotopologue Spectrum Overlap

[14] The isotope fractionation due to spectrum overlap was modeled using the SO_2 cross section reported by *Lyons* [2007, 2008] (Figure 1). These cross sections are based on the high-resolution (0.002 nm) $^{32}SO_2$ cross-section measurements of *Freeman et al*. [1984]. Cross sections for minor isotopologues are estimated by shifting band positions of the $^{32}SO_2$ cross sections. *Lyons* [2007, 2008] used the

Table 1. Results of Flow-through SO_2 Photolysis Experiments. All Isotope Ratios Are Normalized Against That of Starting SO_2

	pSO_2 (mbar)	pN_2 (bar)	Flow Rate (sccm)	$\delta^{33}S$ (‰)	$\delta^{34}S$ (‰)	$\delta^{36}S$ (‰)	$\Delta^{33}S$ (‰)	$\Delta^{36}S$ (‰)
S^0, Front Cell								
S-0705*	0.10	1.0	478	23.21	40.37	65.8	2.56	−11.4
S-0701*	0.11	1.0	233	21.72	37.85	58.1	2.36	−14.0
S-0630	0.29	1.0	86	39.63	69.26	108.5	4.39	−24.0
S-0711	0.29	1.0	86	35.54	61.30	93.5	4.29	−23.4
S-1006*	0.29	1.0	86	36.91	63.36	98.5	4.62	−22.6
S-1011	0.59	1.0	85	48.49	82.91	128.0	6.35	−30.5
S-1020	0.59	1.0	254	48.45	83.92	132.1	5.83	−28.6
S-1021	0.60	1.0	503	48.38	82.90	128.9	6.24	−29.6
S-1007	1.09	1.0	183	71.31	125.41	209.3	8.07	−33.8
S-0708	1.17	1.0	85	63.63	110.96	181.4	7.53	−32.7
S-0713	1.17	1.0	85	63.48	111.07	180.8	7.33	−33.4
S-0706	2.92	1.0	85	71.90	128.03	219.0	7.41	−30.4
S-0714	2.92	1.0	85	76.23	137.15	237.8	7.30	−30.4
S-1013	0.25	0.25	25	33.34	52.64	74.2	6.40	−25.6
S-0905	0.44	0.22	25	52.29	84.76	128.2	9.11	−33.4
S-1012	0.51	0.25	25	50.03	81.00	122.0	8.74	−32.3
S-0907	0.89	0.22	25	71.94	118.67	188.4	11.79	−39.7
S-0906	0.97	0.24	25	75.14	126.95	207.3	10.96	−37.9
S-0830	0.49	0.49	50	50.78	85.37	131.9	7.37	−31.2
S-0902	1.01	0.50	50	69.07	117.35	188.9	9.69	−37.1
S-0921a	2.50	0.50	50	78.43	135.71	230.1	10.02	−34.1
S-0921b	5.00	0.50	50	79.12	138.59	240.4	9.34	−30.7
S^0, Rear Cell								
S-0707R*	0.05[$]	1.0	100	33.22	58.31	96.1	3.50	−15.8
S-0701R*	0.11[$]	1.0	100	46.90	82.89	133.9	4.84	−25.3
S-0630R*	0.29[$]	1.0	100	70.00	126.41	216.0	6.38	−30.1
Residual SO_2								
S-1020	0.59	1.0	254	−1.13	−2.16	−3.9	−0.01	0.2
S-1021	0.60	1.0	503	−0.63	−1.17	−2.0	−0.02	0.2
SO_3 Front Cell								
S-0705	0.10	1.0	478	6.88	12.75	21.6	0.33	−2.7
S-1025	0.58	1.0	86	9.40	17.92	32.7	0.21	−1.6
S-1020	0.59	1.0	254	11.27	21.41	38.2	0.30	−2.8
S-1021	0.60	1.0	503	10.25	19.34	34.1	0.33	−2.9
S-0708	1.17	1.0	85	12.21	23.03	41.1	0.41	−3.0
S-0706*	2.92	1.0	85	10.02	18.72	34.5	0.42	−1.3
SO_3 Rear Cell								
S-0705R	0.10	1.0	100	5.31	9.88	17.1	0.23	−1.7
S-0701R*	0.11	1.0	100	2.27	4.32	7.7	0.05	−0.5

*:microvolume analysis
[$]:These are pSO2 of the front cell. Rear cell pSO2 is held constant at 0.1 mbar

energy shift parameters adapted and extrapolated from ab-initio model study of *Ran et al.* [2007]. Figure 3 compares the isotopologue shift parameters from *Lyons* [2008] and *Ran et al.* [2007] as well as those from ab-initio wave-packet model calculation [*Tokue and Nanbu*, 2010], and experimental measurement [*Danielache et al.*, 2008]. The isotope shift parameters used in this and previous studies agree well with the latest theoretical model by *Tokue and Nanbu* [2010], but experimental data by *Danielache et al.* [2008] show smaller magnitude energy shifts compared to theoretical values. A smaller isotope shift would produce a smaller effect of isotopologue self-shielding due to a higher degree of overlap in the fine vibrational structures.

[15] Following previous studies [e.g., *Lyons*, 2008; *Ueno et al.*, 2009], photolysis quantum yields for $^{32}SO_2$ are assumed to be wavelength (but not isotopologue) dependent above 205 nm and assumed to be unity below 205 nm [*Okazaki et al.* 1997]. The lamp output power (F_{Xe}) was approximated from the manufacturer's data sheet as a function of wavelength (λ in nm):

$$F_{xe} = 0.11 \cdot 1.6 \cdot [14 - 9 \cdot \exp(-0.013/(\lambda - 200))] \quad (\mathrm{mW/nm}). \tag{4}$$

[16] The first and second factors are to correct the efficiency of the condenser (F/1) and rear reflector, respectively. Transmission of quartz windows (τ_w) are measured and fitted as:

$$\tau_w = 0.93 - 6.79 \cdot \exp(-0.027 \cdot \lambda). \tag{5}$$

[17] Total photolysis rates for each isotopologue are derived by integrating over wavelength between 190 and 220 nm and over the pathlength (15 cm) of the flow-through reactor. The major sources of error are the spectrum shape of the Xe lamp, and absorption by the optics and Schumann–Runge band of O_2 in the optical path (which is applicable for wavelengths shorter than 195 nm) [*Whitehill and Ono*, 2012]. The estimated fractionation factor, however, is only a weak function of spectrum shape of the incident light [*Lyons*, 2007]. The overall magnitude of the photon flux affects photolysis yield

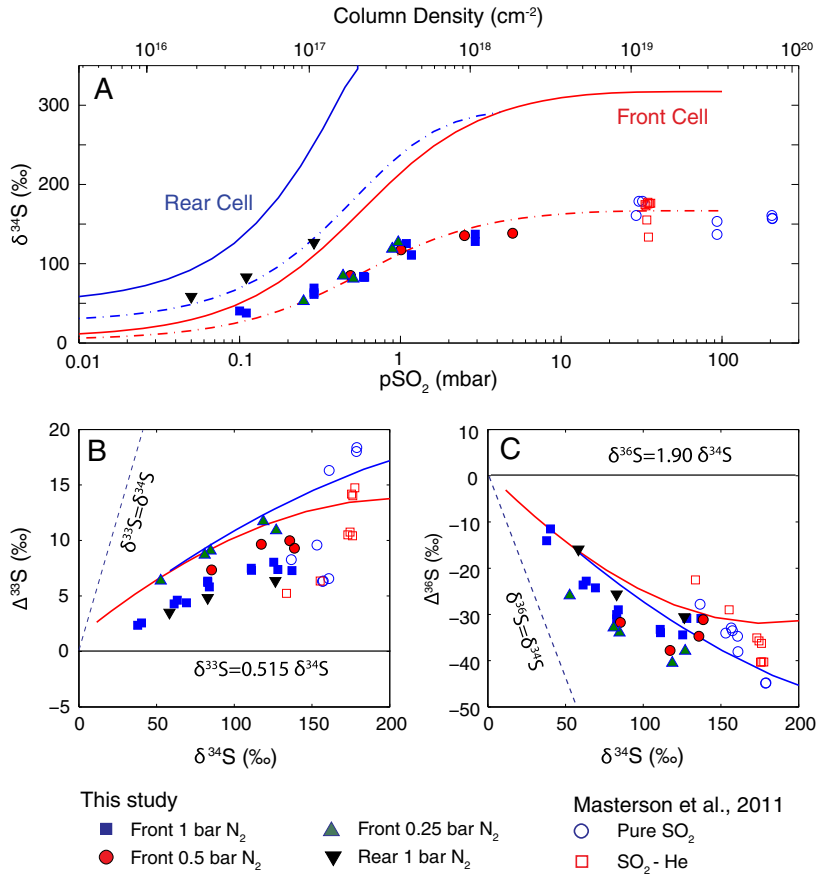

Figure 4. Results of the SO_2 photolysis experiments in this study as a function of pSO_2 and pN_2 (closed symbols). Also shown are model results (solid lines) and results from static cell experiments by *Masterson et al.* [2011] (open symbols) from which data for pSO_2 of >750 mbar are excluded. (A) $\delta^{34}S$ of the product S^0 as a function of pSO_2 and model calculations of self-shielding using the red-shifted isotopologue cross sections of *Lyons* [2007]. Red and blue solid lines represent model results for the front cell and rear cell (pSO_2 of the rear cell was at 0.1 mbar); dashed lines are the same model results for which the magnitude of the $\delta^{34}S$ values were reduced by a factor of 1.9. (B) $\delta^{34}S$ versus $\Delta^{33}S$ and (C) $\delta^{34}S$ versus $\Delta^{36}S$ of the product S^0. The dashed and solid line in Figures 4-B and 4-C represent slopes expected for an ideal self-shielding ($\delta^{33}S = \delta^{34}S = \delta^{36}S$) and wholly mass-dependent fractionation ($\delta^{33}S/0.515 \simeq \delta^{34}S \simeq \delta^{36}S/1.9$), respectively.

but not isotope fractionation. We did not use the cross section from *Danielache et al*. [2008]. As discussed in *Whitehill and Ono* [2012], the cross section from *Danielache et al*. [2008] predicts negative $\Delta^{33}S$ values under the light spectrum of Xe lamp, which is not reproduced by laboratory Xe lamp SO_2 photolysis experiments.

[18] Self-shielding of $^{32}SO_2$, *in an ideal case*, is expected to fractionate all the minor isotopes at the same magnitude. The isotope composition of the resulting product would follow $\delta^{33}S \simeq \delta^{34}S \simeq \delta^{36}S$. This is only true, however, when there is no spectrum overlap between major and minor isotope absorption lines, and when the underlying continuum is very weak, such as for the $^{12}C^{16}O$ absorption band at 105.2 nm. In the case of SO_2 in the 190 to 220 nm range, the magnitude of isotope shift is relatively small compared to the peak width of individual vibrational bands (Figure 1-A and 1-B), and a substantial continuum is present at laboratory and atmospheric temperatures. These significant spectrum overlaps among different SO_2 isotopologue lines cause *mutual shielding* (e.g., $^{32}SO_2$ shielding $^{34}SO_2$), which contributes mass-dependent fractionation. Due to a combination of self- and mutual-shielding effects, spectrum overlaps produce an isotope fractionation pattern that falls between ideal self-shielding ($\delta^{33}S \simeq {}^{34}S \simeq \delta^{36}S$) and mass-dependent fractionation (i.e., $\delta^{33}S/0.515 \simeq \delta^{34}S \simeq \delta^{36}S/1.9$) (Lyons 2009).

3. Results

[19] Elemental sulfur products (S^0) are characterized by large $\delta^{34}S$ values, as high as 140 ‰, and significant $\Delta^{33}S$ and $\Delta^{36}S$ anomalies up to 11.7 ‰ and −40.5 ‰, respectively (Table 1; Figure 4). The magnitude of the $\delta^{34}S$ fractionation is a strong function of pSO_2, increasing with increasing SO_2 column density (Figure 4-A). The results for high pSO_2 experiments ($pSO_2 > 2.5$ mbar) closely match those of static cell experiments by *Masterson et al*. [2011]. Different pressures of nitrogen bath gas (0.25, 0.5, and 1 bar pN_2) produced similar $\delta^{34}S$ values (Figure 4-A). The pN_2, however, affects the relationship between the two isotope fractionation factors, as lower pN_2 produces higher $\delta^{33}S/\delta^{34}S$ ratios (0.57 to 0.64 for 1 to 0.25 bar N_2, respectively) and lower $\delta^{36}S/\delta^{34}S$ values (1.41 to 1.68 for 1 to 0.25 bar N_2, respectively) (Figures 4-B and 4-C). When photochemical cells are placed in series, the rear cell (held at 0.1 mbar pSO_2) consistently yields larger $\delta^{34}S$ values compared to the front cell. The rear cell did not produce a sufficient quantity of S^0 for isotope analysis when the front cell pSO_2 was higher than 0.3 mbar, since the majority of photons were absorbed in the front cell.

[20] Figure 4 also shows the results of the model calculation to be compared with experimental results. The contribution of spectrum overlap is expected for pSO_2 ranging from 0.01 mbar to 10 mbar. Above 10 mbar pSO_2 (column density 10^{18} molecules cm^{-2}), the value of $\delta^{34}S$ reaches the high pSO_2 limit (Figure 4-A). The model calculation and experimental results [including those by *Masterson et al*., 2011] show this saturation effect at high pSO_2, which is expected purely from spectrum overlap. The agreement, however, is not quantitative since the model significantly overestimates the $\delta^{34}S$ effect by a factor 1.9. Dashed lines in Figure 4-A represent the modeled $\delta^{34}S$ values multiplied by the factor 1/1.9 to show this difference. Possible causes of this discrepancy will be discussed.

[21] The model and experimental results agree well for $\delta^{33}S/\delta^{34}S$ and $\delta^{36}S/\delta^{34}S$ ratios; both show isotope fractionation is rather closer to mass-dependent fractionation ($\delta^{33}S/0.515 \simeq \delta^{34}S \simeq \delta^{36}S/1.9$) than *ideal* self-shielding ($\delta^{33}S \simeq \delta^{34}S \simeq \delta^{36}S$) (Figures 4-B and 4-C). This is an expected result due to the significant spectrum overlap among various isotopologue of SO_2 (i.e., mutual shielding) (Figure 1-B) [*Lyons*, 2009]. The experimental results yield $\delta^{33}S/\delta^{34}S$ ratios from 0.57 to 0.64 and $\delta^{36}S/\delta^{34}S$ ratios from 1.41 to 1.68. These experimental values agree well with the model results, which show $\delta^{33}S/\delta^{34}S$ from 0.55 to 0.67 and $\delta^{36}S/\delta^{34}S$ from 1.61 to 1.85. We cannot model the effect of pN_2, as pressure-broadening parameters have not been reported for the 190–220 nm regions.

4. Discussion

4.1. Source of S-MIF During Laboratory SO_2 Photolysis in the 190 to 220 nm Region

[22] The following reactions represent the photolysis of SO_2 under our experimental conditions:

$$SO_2 + h\nu(190 \text{ to } 220\,\text{nm}) \rightarrow SO + O \quad \text{(R1)}$$

$$SO_2 + O + M \rightarrow SO_3 + M, \quad \text{(R2)}$$

$$SO_3 + SO \rightarrow 2SO_2 \quad \text{(R3)}$$

$$SO + SO \rightarrow S + SO_2 \quad \text{(R4)}$$

$$SO + O + M \rightarrow SO_2 + M \quad \text{(R5)}$$

$$SO + h\nu \rightarrow S + O \quad \text{(R6)}$$

where M is the third body molecule (N_2 in our experiments) [*Farquhar et al*., 2001; *Okabe*, 1978]. Reactions (R2), (R3), and (R4) are favored under high pSO_2 (> ca. 1 mbar), while (R5) and (R6) become important in low pSO_2 experiments. Atomic sulfur from reactions (R4) or (R6) polymerizes and forms S^0 aerosols. The above reactions do not include the excitation of SO_2 by radiation in the 240 to 340 nm region ($^1A_2$, $^1B_1 \leftarrow X\ ^1A_1$), since the resulting low-energy excited states are rapidly quenched by N_2 [*Sidebottom et al*., 1972; *Calvert et al*., 1978; *Lyons*, 2009; *Whitehill and Ono*, 2012]. Previous static cell experiments used a 200 ± 35 nm band-pass filter to isolate the photochemistry of SO_2 excited in the 190 to 220 nm versus the 240 to 340 nm absorption region [*Whitehill and Ono*, 2012]. We did not use the band-pass filter in this study because it would significantly limit the number of available photons (maximum transmission of the band-pass filter is 30%). The isotope pattern observed in this study (large $\delta^{34}S$ values and small $\delta^{33}S/\delta^{34}S$, negative $\Delta^{36}S/\Delta^{33}S$ values) is consistent with the 190 to 220 nm excitation band origin of the S-MIF. Isotope signatures for the 240–340 nm band ($\delta^{33}S/\delta^{34}S > 1$ and $\Delta^{36}S/\Delta^{33}S = 0.64$) [*Whitehill and Ono*, 2012] are distinctly different from the isotope pattern observed in this study, suggesting only a minor (if not entirely absent) contribution from the excitation in the 240 to 340 nm regions.

[23] The qualitative agreement between measured S-MIF in the elemental S products and estimated S-MIF from spectrum overlap suggests a critical and significant contribution

of isotopologue self-shielding for the observed S-MIF during SO_2 photolysis under 190 to 220 nm excitation. Similarity between cross-section calculations and experimental results include (1) small S-MIF (and small $\delta^{34}S$ values) at low pSO_2, increasing with increasing pSO_2 and reaching saturation at an SO_2 column density of 10^{18} molecules cm^{-2}, (2) $\delta^{33}S/\delta^{34}S$ and $\delta^{36}S/\delta^{34}S$ relationships, and (3) dual-cell experiments showing the change of S-MIF in the rear cell by changing only the pSO_2 of the front cell. The model calculation, however, overestimates the $\delta^{34}S$ value by a factor of 1.9. This could be, in part, due to different temperatures for the cross-section measurement [213 K, *Freeman et al*., 1984] compared to our photochemical experiment (ca. 300 K), as well as a possible effect of chemistry following photolysis (i.e., R2 to R6) as discussed below. Higher temperature may affect the population of rotational energy levels and affect both the width and the amplitude of the absorption bands.

[24] Our experimental results indicate that $\Delta^{33}S/\delta^{34}S$ and $\Delta^{36}S/\delta^{34}S$ relationships also depend on pN_2 (low pN_2 favors larger $\Delta^{33}S$ and $\Delta^{36}S$ anomalies), consistent with the results of static cell experiments for pSO_2 with added helium [*Masterson et al*., 2011]. If observed S-MIF is indeed predominantly caused by self-shielding, the effect of bath gas pressure can be explained by pressure broadening of the absorption features at the low-energy side of the spectrum (>210 nm), where the fluorescence lifetime of the excited state SO_2 is comparable to the collision frequency [*Katagiri et al*., 1997]. Measurements of the pressure-broadening factor may provide key insights into the effect of bath gas on the S-MIF pattern. *Masterson et al*. [2011] observed decreasing magnitude of MIF at high pSO_2 (>30 mbar) by static cell experiments. While this may appear contradictory to our results showing smaller magnitude MIF at lower pSO_2 (<1 mbar), it is likely that the excess SO_2 at very high pSO_2 (>30 mbar) would act as a bath gas, resulting in the observed lower S-MIF anomaly.

[25] The observed pSO_2 dependence provides critical insights into the potential contribution to MIF from mechanisms other than self-shielding. The S-MIF may originate—independent of a self-shielding mechanism—from quantum efficiencies for photolysis that are isotopologue dependent, such as nonadiabatic surface crossings [*Zmolek et al*., 1999; *Muskatel et al*., 2011] or from isotopologue-dependent absorption line strengths [*Danielache et al*., 2008]. Our experimental results suggest that these two effects make only a minor contribution to S-MIF ($\Delta^{33}S < 2.5$ ‰) under our experimental conditions, because both mechanisms should be effective even at the lowest optical density. This does not, however, exclude the possibility of S-MIF in nature at much lower pSO_2. One also needs to be cautious in applying experimental results to natural conditions because sulfur isotope exchange reactions, such as,

$$^{32}SO_2 + {}^{x}SO \rightarrow {}^{x}SO_2 + {}^{32}SO, \quad \text{(R7)}$$

may be important and effectively minimize the S-MIF signatures in SO (x = 33, 34, or 36). Isotope exchange kinetics, however, are expected to be first order with respect to pSO_2. The saturation of ^{34}S fractionation at 10 mbar pSO_2 (Figure 4-A) suggests that the isotope exchange reaction (R7) is relatively slow: if R7 were fast, one would expect to see decreasing $\delta^{34}S$ with increasing pSO_2 above 10 mbar.

[26] Other than SO_2 photolysis itself (R1), any one of the reactions above (R2 to R6) could contribute to mass-dependent or mass-independent fractionation. Our experimental results can be used to eliminate some reactions from all the potential S-MIF source reactions. Small isotope effects at low pSO_2 suggest that (R5) and (R6) are not the main source of MIF, as these two reactions are favored under low pSO_2. The SO_2 oxidation reaction (R2) is mass dependent because the product SO_3 is fractionated only mass dependently (Table 1). The reactions SO + SO_3 (R3) or SO + SO (R4) are potential sources for S-MIF. Results of our experiments cannot fully exclude the possibility of S-MIF during (R3) and (R4). It is difficult to test the possibility, however, without knowing the mechanism and predicted isotope pattern (e.g., $\Delta^{33}S/\delta^{34}S$ or $\Delta^{36}S/\Delta^{33}S$ ratios). The SO + SO reaction (R4) may produce SO-dimer intermediates, of which some of the low electronic states are symmetric, which could potentially produce symmetry-dependent MIF [*Lyons*, 2008]. Symmetry-dependent MIF, in an ideal case, would produce nearly equal enrichment in all minor isotopes (i.e., $\delta^{33}S \simeq 1.04$ $\delta^{34}S \simeq \delta^{36}S$, where the factor 1.04 accounts for the symmetric species with two ^{34}S) and result in the $\Delta^{36}S/\Delta^{33}S$ ratios of −1.6 [*Ono et al*., 2009]. This is much higher than what we have measured.

4.2. Implication for the MIF in SSA

[27] Significant SO_2 isotope self-shielding is expected when the SO_2 column density exceeds ca. 10^{17} molecules cm^{-2} (Figure 4-A). During large explosive volcanic events, such as the Mt. Pinatubo (1991) eruption, the SO_2 column density can reach and exceed these levels. The SO_2 column density following the Pinatubo (1991) eruption initially reached as high as 10^{19} molecules cm^{-2}. Within two weeks, the SO_2 cloud covered an area in excess of 10^{17} km^2 with an SO_2 column density above 10^{17} molecules cm^{-2} [e.g., *Guo et al*., 2004]. Therefore, isotopologue self-shielding is expected to occur during direct photolysis of SO_2 following stratospheric volcanic events. In support of this hypothesis, S-MIF signatures (i.e., $\Delta^{33}S/\delta^{34}S$ and $\Delta^{36}S/\Delta^{33}S$ ratios) produced by our experiments agree well with those for SSA trapped in polar ice [*Savarino et al*., 2003; *Baroni et al*., 2007, 2008] (Figures 5-C and 5-F).

[28] The isotope effect in the 190 to 220 nm region is exclusive to the stratosphere, since radiation in the 190 to 220 nm range is only available above 20 km due to absorption by O_2 and O_3 in this wavelength region [e.g., *Farquhar et al*., 2001]. This is consistent with the observation of S-MIF signatures for SSA exclusively from large stratospheric eruptions. Preservation of the S-MIF signature, however, remains problematic, since reaction with O_2 rapidly oxidizes SO back to SO_2.

$$SO + O_2 \rightarrow SO_2 + O \quad \text{(R8)}$$

Instead of SO_2 photolysis (R1), *Savarino et al*. [2003] suggest that the S-MIF in SSA sourced from photo-oxidation of SO_2:

$$^{*}SO_2 + SO_2 \rightarrow SO_3 + SO \quad \text{(R9)}$$

where $^{*}SO_2$ is excited state SO_2 produced by excitation under 240 to 330 nm absorption bands [*Calvert et al*., 1978; *Chung et al*., 1975; *Savarino et al*., 2003]. Transfer

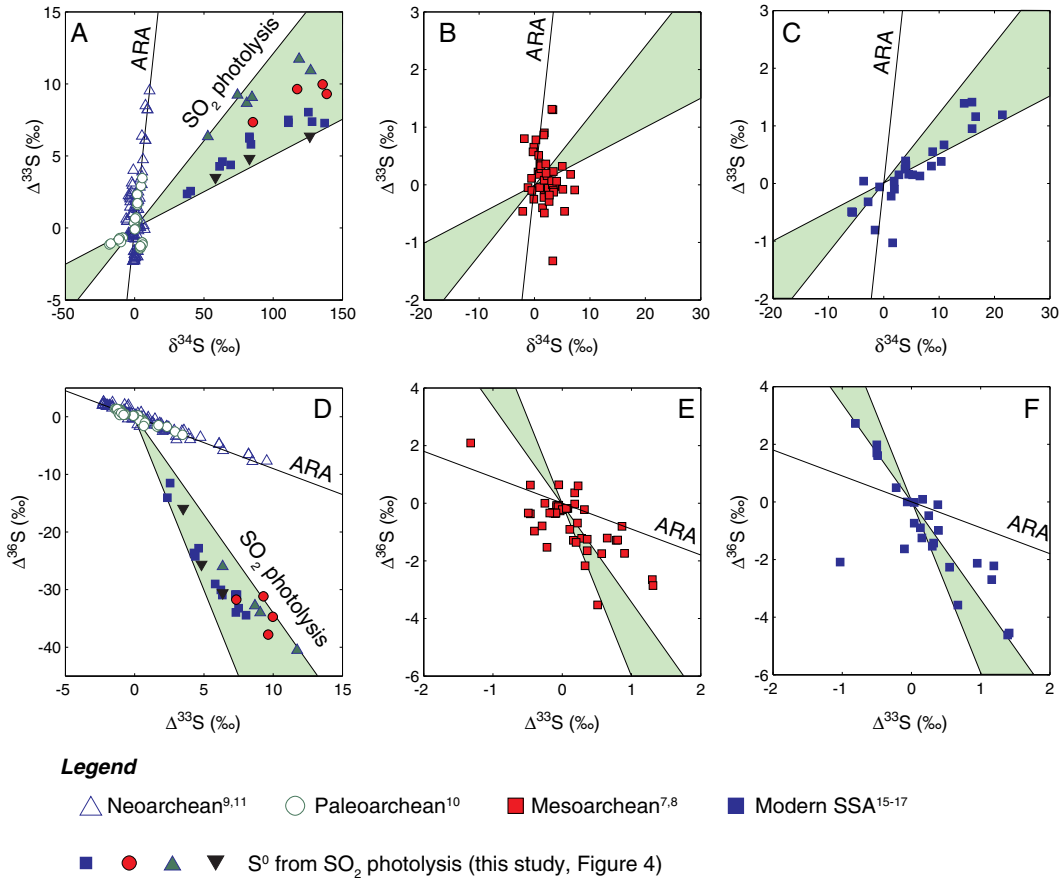

Figure 5. Plot of $\delta^{34}S$ versus $\Delta^{33}S$ (A, B, and C) and $\Delta^{33}S$ versus $\Delta^{36}S$ (D, E, F) for laboratory SO_2 results compared with literature data for Archean rocks and modern SSA. (A and D) Experimental results from this study are compared with data from Neoarchean and Paleoarchean rocks in W. Australia and S. Africa, characterized by Archean Reference Array (ARA), which is shown in dashed lines ($\Delta^{33}S/\delta^{34}S = 0.9$, and $\Delta^{36}S/\Delta^{33}S = -0.9$ and -1.5. The ranges of $\Delta^{33}S/\delta^{34}S$ and $\Delta^{36}S/\Delta^{33}S$ slopes for experimental results, 0.086 ± 0.035 and -4.6 ± 1.3, respectively, are highlighted as light green areas. (B and E) ARA and self-shielding slopes are compared with data from Mesoarchean rocks from 2.8 to 3.2 Ga. (C and F) The slopes are compared with data for modern SSA. Data sources for Archean S-MIF are *Kaufman et al.* [2007], *Zerkle et al.* [2012], *Farquhar et al.* [2007], *Ono et al.* [2006a], *Ono et al.* [2009], and *Ueno et al.* [2008]. Data sources for stratospheric sulfate aerosols are *Savarino et al.* [2003] and *Baroni et al.* [2007, 2008].

of sulfur isotope signatures from $^*SO_2$ to SO_3 would allow preservation of the S-MIF signature in $^*SO_2$. A recent photochemical study, however, showed that the sulfur in SO_3 in reaction (R9) is largely (if not exclusively) derived from ground state SO_2 [*Whitehill and Ono*, 2012]. The study also showed that the 240 to 330 nm excitation band produces positive $\Delta^{36}S/\Delta^{33}S$ values (~0.63) rather than the negative values observed in SSA, suggesting photo-oxidation (R9) is not a likely candidate for S-MIF in modern SSA.

[29] The preservation of SO isotope signatures (rather than through R9), thus, implies the presence of an unknown reaction that preserves the S-MIF signatures in SO. A reaction such as

$$SO + O_2 + M \rightarrow SO_3 + M \quad \text{(R10)}$$

is only postulated by some researchers [*Myerson et al.*, 1957; *Wood and Heicklen*, 1971; *Black et al.*, 1982], but may provide a mechanism to preserve S-MIF signatures. The extent that reaction (R10) may contribute to sulfate formation can be estimated by comparing the kinetics of SO_2 oxidation by OH:

$$SO_2 + OH + M \rightarrow HSO_3 + M \quad \text{(R11)}$$

$$HSO_3 + O_2 \rightarrow SO_3 + HO_2 \quad \text{(R12)}$$

$$SO_3 + H_2O \rightarrow H_2SO_4 \quad \text{(R13)}$$

At steady state with respect to SO, the fraction of SO_3 produced from SO (f_{SO}) is

$$f_{SO} = \frac{J_1 k_{10}}{k_{11}[OH](k_8 + k_{10}[M]) + J_1 k_{10}} \quad (6)$$

where k_8, k_{10}, and k_{11} are the rate constants for R8, R10, and R11, respectively, and J_1 is the photolysis rate of SO_2. As an example of SO_2 photolysis in a stratospheric volcanic

plume, we consider a total SO_2 column depth of 10 DU (2.7×10^{17} cm^{-2}), which is distributed at height 27 ± 7 (FWHM) km [e.g., *Aquila et al.*, 2012]. The model result shows that a rate constant k_{10} of 10^{-36} cm^6/s (which is the maximum rate suggested by *Black et al.* [1982]) can allow R10 to contribute up to 10% of SO_3 formation at above 30 km (Figure 6). A smaller value of k_{10} will decrease this contribution as shown in Figure 6. The maximum $\Delta^{33}S$ value observed for sulfate aerosol in polar ice [1.4 ‰, *Baroni et al.*, 2007] is only 12% of the maximum $\Delta^{33}S$ value observed in this study (11.8 ‰), suggesting that the contribution of SO_2 photolysis of 12% or less can explain the polar ice S-MIF signatures (i.e., $SO_2 + OH$ reaction is still a dominant source of SO_2 oxidation).

[30] The presence of ash, ice particles, and other molecular constituents in the volcanic plume (e.g., HCl, H_2S) could modify sulfur chemistry in several ways. First, the fraction of O_2 in the plume will be somewhat lower than in clean stratospheric air. Second, O_3 and OH will be lower, possibly substantially lower, than in the background stratosphere due to surface reactions on plume particles. Lower OH will decrease the sulfate formation rate by reaction (R11) and increase the fraction of sulfate produced from SO (i.e., the second term in equation (6) increases). Faster conversion of SO to sulfate (R10) versus SO_2 to sulfate (R11) during initial plume chemistry, would be consistent with the observation by *Baroni et al.* [2007] that SSA with $\Delta^{33}S > 0$ was deposited first in Antarctic snow, followed by SSA with $\Delta^{33}S < 0$. Finally, reaction (R10) is likely to have a large activation energy and could be entirely negligible at stratospheric temperatures. Heterogeneous addition of SO and O_2 on ash or ice particles,

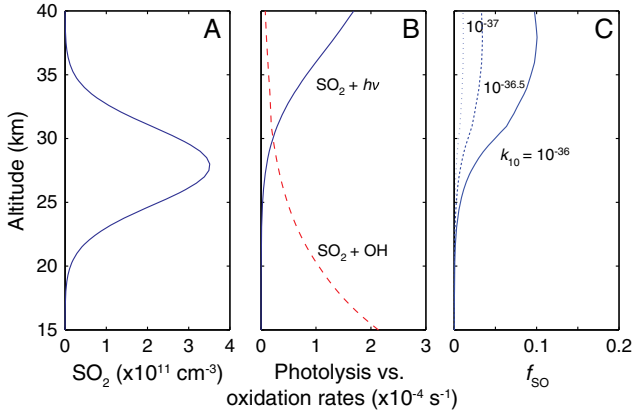

Figure 6. Results of model calculation for stratospheric SO_2 chemistry during the initial stage of a Plinian volcanic eruption. (A) assumed SO_2 number density, (B) SO_2 photolysis rate (J_1) compared with SO_2 oxidation rate (=k_{11}[OH][M]), and (C) modeled value of f_{SO} as a function of k_{10} (10^{-36},$10^{-36.5}$, and 10^{-37} cm^6/s^{-1}). The rate constants, k_8 and k_{11}, are from *Sander et al.* [2006]. Temperature, O_3 and O_2 number densities are from US Standard Atmosphere [*COESA*, 1976], OH number density is assumed to be 8×10^6 cm^{-3} below 31 km, increasing linearly with altitude to 1.6×10^7 cm^{-3} at 40 km following *Jucks et al.* [1998]. Actinic photon flux is from *Rottman et al.* [2006], and the calculation is performed for solar zenith angle of 30°.

$$SO + O_2 \xrightarrow{Ash,Ice} SO_3 \qquad \text{(R14)}$$

could be rapid compared to gas-phase oxidation of SO_2.

[31] Detailed modeling of stratospheric sulfur chemistry is beyond the scope of this study. Understanding the production and preservation of S-MIF signatures will provide a unique constraint on the origin and fate of stratospheric sulfur aerosols, which have a significant impact on global climate by compensating the greenhouse warming effects [*Turco et al.*, 1982; *Robock et al.*, 2008].

4.3. Implication to Archean S-MIF

[32] Some well-preserved Archean rocks show characteristic $\Delta^{33}S/\delta^{34}S$ and $\Delta^{36}S/\Delta^{33}S$ ratios of 0.9 and −0.9, respectively [e.g., *Ono et al.*, 2003; *Kaufman et al.*, 2007; *Zerkle et al.*, 2012]. The ranges of $\Delta^{33}S/\delta^{34}S$ and $\Delta^{36}S/\Delta^{33}S$ ratios produced by our experiments (0.086 ± 0.035 and -4.6 ± 1.3, respectively) do not match these main Archean arrays, suggesting that the main source reaction for Archean S-MIF may not be linked to our experimental results (Figures 4-A and 4-D). It is, however, conceivable that the isotopologue self-shielding could have made a secondary contribution to the structure of $\Delta^{36}S/\Delta^{33}S$ record when high SO_2 column density was achieved after large volcanic eruptions. Studies of rocks from Neoarchean age (2.5 to 2.65 Ga) have shown several stratigraphic intervals with lower $\Delta^{36}S/\Delta^{33}S$ ratios of −1.5 compared to a more common value of −0.9 [*Kaufman et al.*, 2007; *Zerkle et al.*, 2012]. In addition, data for rocks between 3.2 and 2.8 Ga are characterized by relatively small $\Delta^{33}S$ values and with more negative $\Delta^{36}S$ values (Figure 4-E). The cause of these secular changes in the structure of Archean S-MIF has been attributed to a variety of changes in atmospheric chemistry [*Farquhar et al.*, 2007], including ephemeral oxidation [*Ono et al.*, 2006a; *Ohmoto et al.*, 2006; *Kaufman et al.*, 2007], the development of organic haze [*Domagal-Goldman et al.*, 2008; *Zerkle et al.*, 2012], or changes in volcanic gas SO_2/H_2S ratios [*Halevy et al.*, 2010]. The results of this study suggest that the observed $\Delta^{36}S/\Delta^{33}S$ trend can be explained by a combination of the main Archean S-MIF reaction (with $\Delta^{36}S/\Delta^{33}S \approx -0.9$) and the isotope self-shielding due to increased volcanic SO_2 loading (with $\Delta^{36}S/\Delta^{33}S \approx -4.6$). In particular, the Mesoarchean increase of SO_2 loading is consistent with abundant detrital and diagenetic pyrite in the Witwatersrand Supergroup, despite presumably low sulfate levels of the Archean oceans [*Habicht et al.*, 2002]. Increased SO_2 loading would have had significant consequences on the early Earth's climate, because a temporal increase of sulfate in surface environments would suppress microbial methanogenesis by competing for H_2 with sulfate reducers [*Lovley and Klug*, 1983]. The collapse of methanogens would have triggered the oldest known glaciations in the Witwatersrand-Pongola basins at ca. 2.9 Ga [*Young et al.*, 1998; *Ono et al.*, 2006a].

5. Conclusion

[33] Sulfur isotope effects during the UV photolysis of SO_2 under a broadband light source were investigated with a flow-through photochemical reactor. The S-MIF signature and the $\delta^{34}S$ values of S^0 products increase with increasing SO_2 pressure, but saturate at a column density of 10^{18} molecules cm^{-2}. The SO_2 column density dependence, large $\delta^{34}S$

values, and $\Delta^{33}S/\delta^{34}S$ and $\Delta^{36}S/\delta^{34}S$ relationships suggest an important contribution of isotopologue self-shielding to the observed mass-independent isotope effect. Results from dual-cell experiments further support this conclusion. The measured isotope pattern, in particular the $\Delta^{36}S/\Delta^{33}S$ ratios, show good agreement with data for SSA, suggesting that photolysis of SO_2 in the 190 to 220 nm region following large volcanic events could be the dominant source of the modern S-MIF in SSA. This implies there is a currently unknown mechanism for preserving the isotope signature of SO formed from SO_2 photolysis in the stratosphere. Although the results do not agree with the main Archean S-MIF array, SO_2 self-shielding could have contributed to the $\Delta^{36}S/\Delta^{33}S$ variations during parts of the Archean.

[34] **Acknowledgments.** Authors thank William J. Olszewski and Kat Thomas for assistance in sulfur isotope analysis, and Eliza Harris for proofreading. This work was supported by the NASA Exobiology Program, Grant No. NNX10AR85G to Ono and NNX10AR80G to Lyons. The authors also thank Sebastian Danielache and two anonymous reviewers for constructive comments to the earlier version of the manuscript.

References

Aquila, V., L. D. Oman, R. S. Stolarski, P. R. Colarco, and P. a. Newman (2012), Dispersion of the volcanic sulfate cloud from a Mount Pinatubo–like eruption, *J. Geophy. Res.*, *117*(D6), 1–14, doi:10.1029/2011JD016968.

Baroni, M., J. Savarino, J. Cole-Dai, V. K. Rai, and M. H. Thiemens (2008), Anomalous sulfur isotope compositions of volcanic sulfate over the last millennium in Antarctic ice cores, *J. Geophys. Res.*, *113*(D20), 1–12, doi:10.1029/2008JD010185.

Baroni, M., M. H. Thiemens, R. J. Delmas, and J. Savarino (2007), Mass-independent sulfur isotopic compositions in stratospheric volcanic eruptions, *Science*, *315*(5808), 84–87, doi:10.1126/science.1131754

Black, G., R. L. Sharpless, and T. G. Slanger (1982), Rate coefficients at 298 K for SO reactions with O_2, O_3, and NO_2, *Chem. Phys. Lett.*, *90*(1), 55–58. doi:10.1016/0009-2614(82)83324-1.

Calvert, J., F. Su, J. Bottenheim, and O. Strausz (1978), Mechanism of the homogeneous oxidation of sulfur dioxide in the troposphere, *Atmos. Environ.*, *12*, 197–226.

Chung, K., Calvert, J. G., and Bottenheim, J. W. (1975), The photochemistry of sulfur dioxide excited within its first allowed band (3130 Å) and the "forbidden" band (3700–4000 Å), *Int. J. Chem. Kinet.*, *7*(2), 161–182, doi:10.1002/kin.550070202.

COESA (1976), U.S. Standard Atmosphere, 1976, p. 227, NOAA.

Coplen, T. B. (2011), Guidelines and recommended terms for expression of stable-isotope-ratio and gas-ratio measurement results, *Rapid Commun. Mass Spectrom.*, *25*(17), 2538–2560, doi:10.1002/rcm.5129.

Danielache, S. O., C. Eskebjerg, M. S. Johnson, Y. Ueno, and N. Yoshida (2008), High-precision spectroscopy of ^{32}S, ^{33}S, and ^{34}S sulfur dioxide: Ultraviolet absorption cross sections and isotope effects, *J. Geophys. Res.*, *113*(D17), 1–14, doi:10.1029/2007JD009695.

Domagal-Goldman, S. D., J. F. Kasting, D. V. Johnston, and J. Farquhar (2008), Organic haze, glaciations and multiple sulfur isotopes in the Mid-Archean Era, *Earth Planet. Sci. Lett.*, *269*(1–2), 29–40, doi:10.1016/j.epsl.2008.01.040.

Farquhar, J., H. Bao, and M. H. Thiemens (2000a), Atmospheric influence of Earth's earliest sulfur cycle, *Science*, *289*(5480), 756–758, doi:10.1126/science.289.5480.756.

Farquhar, J., M. Peters, D. V. Johnston, H. Strauss, A. Masterson, U. Wiechert, and A. J. Kaufman (2007), Isotopic evidence for Mesoarchaean anoxia and changing atmospheric sulphur chemistry, *Nature*, *449*(7163), 706–709, doi:10.1038/nature06202.

Farquhar, J., J. Savarino, S. Airieau, and M. H. Thiemens (2001), Observation of wavelength-sensitive mass-independent sulfur isotope effects during SO_2 photolysis: Implications for the early atmosphere, *J. Geophys. Res.*, *106*(E12), 32829–32832.

Farquhar, J., J. Savarino, T. L. Jackson, and M. H. Thiemens (2000b), Evidence of atmospheric sulphur in the martian regolith from sulphur isotopes in meteorites, *Nature*, *404*(6773), 50–52, doi:10.1038/35003517.

Forrest, J., and L. Newman (1977), Silver-110 microgram sulfate analysis for the short time resolution of ambient levels of sulfur aerosol, *Anal. Chem.*, *49*(11), 1579–1584.

Freeman, D., K. Yoshino, J. Esmond, and W. Parkinson (1984), High resolution absorption cross section measurements of SO_2 at 213 K in the wavelength region 172–240 nm, *Planet. Space Sci.*, *32*(9), 1125–1134, doi:10.1016/0032-0633(84)90139-9.

Gao, Y. Q., and R. Marcus (2001), Strange and unconventional isotope effects in ozone formation, *Science*, *293*(5528), 259–263, doi:10.1126/science.1058528.

Gröger, J., J. Franke, and K. Hamer (2009), Quantitative recovery of elemental sulfur and improved selectivity in a chromium reducible sulfur distillation, *Geostand. Geoanal. Res.*, *33*(1), 17–27. doi:10.1111/j.1751-908X.2009.00922.x

Guo, S., G. Bluth, W. Rose, and I. Watson (2004), Re-evaluation of SO_2 release of the 15 June 1991 Pinatubo eruption using ultraviolet and infrared satellite sensors, *Geochem. Geophys.*, *5*(4), 1–31, doi:10.1029/2003GC000654.

Habicht, K. S., M. Gade, B. Thamdrup, P. Berg, and D. E. Canfield (2002), Calibration of sulfate levels in the archean ocean., *Science*, *298*(5602), 2372–2374, doi:10.1126/science.1078265.

Halevy, I., D. V. Johnston, and D. P. Schrag (2010), Explaining the structure of the Archean mass-independent sulfur isotope record, *Science*, *329*(5988), 204–207, doi:10.1126/science.1190298.

Jucks, K., D. Johnson, and K. Chance (1998). Observations of OH, HO_2, H_2O, and O_3 in the upper stratosphere: Implications for photochemistry. *Geophys. Res. Lett.*, *25*(21), 3935–3938.

Kaiser, J., T. Röckmann, and C. A. M. Brenninkmeijer (2004), Contribution of mass-dependent fractionation to the oxygen isotope anomaly of atmospheric nitrous oxide, *J. Geophys. Res.*, *109*(D3), 1–11, doi:10.1029/2003JD004088

Katagiri, H., T. Sako, A. Hishikawa, T. Yazaki, K. Onda, K. Yamanouchih, and K. Yoshino (1997), Experimental and theoretical exploration of photodissociation of SO_2 via the C^1B_2 state: Identification of the dissociation pathway, *J. Mol. Struct.*, *413–414*, 589–614.

Kaufman, A. J., D. V. Johnston, J. Farquhar, A. L. Masterson, T. W. Lyons, S. Bates, A. D. Anbar, G. L. Arnold, J. Garvin, and R. Buick (2007), Late Archean biospheric oxygenation and atmospheric evolution, *Science*, *317*(5846), 1900–1903, doi:10.1126/science.1138700.

Lin, Y., M. S. Sim, and S. Ono (2011). Multiple-sulfur isotope effects during photolysis of carbonyl sulfide, *Atmos. Chem. Phys.*, *11*(19), 10283–10292, doi:10.5194/acp-11-10283-2011.

Lovley, D., and M. Klug (1983), Sulfate reducers can outcompete methanogens at freshwater sulfate concentrations, *Appl. Environ. Microbiol.*, *45*(1), 187–192.

Lyons, J. R. (2007), Mass-independent fractionation of sulfur isotopes by isotope-selective photodissociation of SO_2, *Geophys. Res. Lett.*, *34*(22), 1–5, doi:10.1029/2007GL031031.

Lyons, J. R. (2008), Photolysis of long-lived predissociative molecules as a source of mass-independent isotope fractionation: The example of SO_2, *Adv. Quantum Chem.*, *55*(07), 57–74, doi:10.1016/S0065-3276(07)00205-5.

Lyons, J. R. (2009), Atmospherically-derived mass-independent sulfur isotope signatures, and incorporation into sediments, *Chem. Geol.*, *267*, 164–174, doi:10.1016/j.chemgeo.2009.03.027.

Masterson, A. L., J. Farquhar, and B. Wing (2011), Sulfur mass-independent fractionation patterns in the broadband UV photolysis of sulfur dioxide: Pressure and third body effects, *Earth Planet. Sci. Lett.*, *306*(3–4), 253–260, doi:10.1016/j.epsl.2011.04.004.

Muskatel, B. H., F. Remacle, M. H. Thiemens, and R. D. Levine (2011), On the strong and selective isotope effect in the UV excitation of N_2 with implications toward the nebula and Martian atmosphere, *Proc. Natl. Acad. Sci. U.S.A.*, *108*(15), 6020–6025, doi:10.1073/pnas.1102767108.

Myerson, A., F. Taylor, and P. Hanst (1957), Ultraviolet absorption spectra and the chemical mechanism of CS_2-O_2 explosions, *J. Chem. Phys.*, *26*(5), 1309–1320, doi:10.1063/1.1743513.

Ohmoto, H., Y. Watanabe, H. Ikemi, S. R. Poulson, and B. E. Taylor (2006), Sulphur isotope evidence for an oxic Archaean atmosphere, *Nature*, *442*(7105), 908–911, doi:10.1038/nature05044.

Okabe, H. (1978), Photochemistry of Small Molecules, John Wiley & Sons, New York.

Okazaki, A., T. Ebata, and N. Mikami (1997), Degenerate four-wave mixing and photofragment yield spectroscopic study of jet-cooled SO_2 in the C^1B_2 state: Internal conversion followed by dissociation in the X state, *J. Chem. Phys.*, *107*, 8752–8758.

Ono, S., N. J. Beukes, and D. Rumble (2009), Origin of two distinct multiple-sulfur isotope compositions of pyrite in the 2.5 Ga Klein Naute Formation, Griqualand West Basin, South Africa, *Precambrian Res.*, *169*(1–4), 48–57, doi:10.1016/j.precamres.2008.10.012.

Ono, S., J. L. Eigenbrode, A. A. Pavlov, P. Kharecha, D. Rumble, J. F. Kasting, and K. H. Freeman (2003), New insights into Archean sulfur cycle from mass-independent sulfur isotope records from the Hamersley Basin, Australia, *Earth Planet. Sci. Lett.*, *213*(1–2), 15–30, doi:10.1016/S0012-821X(03)00295-4.

Ono, S., N. S. Keller, O. Rouxel, and J. C. Alt (2012), Sulfur-33 constraints on the origin of secondary pyrite in altered oceanic basement. *Geochim. Cosmochim. Acta*, *87*, 323–340. doi:10.1016/j.gca.2012.04.016

Ono, S., D. Rumble, N. J. Beukes, and M. L. Fogel (2006a), Early evolution of atmospheric oxygen from multiple-sulfur and carbon isotope records of the 2.9 Ga Mozaan Group of the Pongola Supergroup, Southern Africa, *S. Afr. J. Geol.*, *109*(1–2), 97–108, doi: 10.2113/gssajg.109.1-2.97.

Ono, S., B. Wing, D. V. Johnston, J. Farquhar, and D. Rumble (2006b), Mass-dependent fractionation of quadruple stable sulfur isotope system as a new tracer of sulfur biogeochemical cycles, *Geochim. Cosmochim. Acta*, *70*(9), 2238–2252, doi:10.1016/j.gca.2006.01.022

Pavlov, A. A., and J. F. Kasting (2002), Mass-independent fractionation of sulfur isotopes in Archean sediments: Strong evidence for an anoxic Archean atmosphere, *Astrobiology*, *2*(1), 27–41.

Pavlov, A. A., M. J. Mills, and O. B. Toon (2005), Mystery of the volcanic mass-independent sulfur isotope fractionation signature in the Antarctic ice core, *Geophys. Res. Lett.*, *32*(12), L12816, doi:10.1029/2005GL022784.

Ran, H., D. Xie, and H. Guo (2007), Theoretical studies of absorption spectra of SO_2 isotopomers, *Chem. Phys. Lett.*, *439*(4–6), 280–283, doi:10.1016/j.cplett.2007.03.103.

Robock, A., L. Oman, and G. L. Stenchikov (2008), Regional climate responses to geoengineering with tropical and Arctic SO_2 injections, *J. Geophys. Res.*, *113*(D16), 1–15, doi:10.1029/2008JD010050.

Rottman, G. J., T. N. Woods, and W. McClintock (2006). SORCE solar UV irradiance results, *Adv. Space Res.*, *37*(2), 201–208, doi:10.1016/j.asr.2005.02.072.

Sander, S., D. Golden, M. Kurylo, and G. Moortgat (2006), Chemical Kinetics and photochemical data for use in atmospheric studies: evaluation Number 14, Jet Propulsion Laboratory, Pasadena, CA.

Savarino, J., A. Romero, J. Cole-Dai, and S. Bekki (2003), UV induced mass-independent sulfur isotope fractionation in stratospheric volcanic sulfate, *Geophys. Res. Lett.*, *30*(21), 9–12, doi:10.1029/2003GL018134.

Sidebottom, H. W., C. C. Badcock, G. E. Jackson, J. G. Calvertl, G. W. Reinhardt, and E. K. Damon (1972), Photooxidation of sulfur dDioxide, *Environ. Sci. Technol.*, *6*(1), 72–79.

Tokue, I., and S. Nanbu (2010), Theoretical studies of absorption cross sections for the C^1B_2 X^1A_1 system of sulfur dioxide and isotope effects, *J. Chem. Phys.*, *132*(2), 024301, doi:10.1063/1.3277191.

Turco, R., R. Whitten, and O. Toon (1982), Stratospheric aerosols: Observation and theory, *Rev. Geophy. Space Phys.*, *20*(2), 233–279.

Ueno, Y., M. S. Johnson, S. O. Danielache, C. Eskebjerg, A. Pandey, and N. Yoshida (2009), Geological sulfur isotopes indicate elevated OCS in the Archean atmosphere, solving faint young sun paradox, *Proc. Natl. Acad. Sci. U.S.A.*, *106*(35), 14784–14789, doi:10.1073/pnas.0903518106.

Ueno, Y., S. Ono, D. Rumble, and S. Maruyama (2008), Quadruple sulfur isotope analysis of ca. 3.5 Ga Dresser Formation: New evidence for microbial sulfate reduction in the early Archean, *Geochim. Cosmochim. Acta*, *72*(23), 5675–5691, doi:10.1016/j.gca.2008.08.026

Urey, H. C. (1947), The thermodynamic properties of isotopic substances, *J. Chem. Soc.*, 562–581.

Ustinov, V. I., V. A. Grinenko, and S. G. Ivanov (1988), Sulfur isotope effect in the photolysis of SO_2, *Russ. Chem. Bull.*, *37*(5), 1052.

Whitehill A. R., and S. Ono (2012) Excitation band dependence of sulfur isotope mass-independent fractionation during photochemistry of sulfur dioxide using broadband light sources, *Geochim. Cosmochim. Acta*, *94*, 238–253. doi:10.1016/j.gca.2012.06.014.

Wood, W. P., and J. Heicklen (1971). Kinetics and mechanism of the carbon disulfide-oxygen explosion. *J. Phys. Chem.*, *75*(7), 861–866. doi:10.1021/j100677a003.

Young, G. M., V. von Brunn, D. J. C. Gold, and W. E. Minter (1998), Earth's oldest reported glaciation: Physical and chemical evidence from the Archean Mozaan Group (~2.9 Ga) of South Africa, *J. Geol.*, *106*, 523–538.

Zerkle, A. L., M. W. Claire, S. D. Domagal-Goldman, J. Farquhar, and S. W. Poulton (2012), A bistable organic-rich atmosphere on the Neoarchaean Earth, *Nat. Geosci.*, *5*(4), 1–5, doi:10.1038/ngeo1425.

Zmolek, P., X. Xu, T. Jackson, M. H. Thiemens, and W. C. Trogler (1999), Large mass independent sulfur isotope fractionations during the photopolymerization of $^{12}CS_2$ and $^{13}CS_2$, *J. Phys. Chem. A*, *103*(15), 13–16.